Entanglement entropy of Bell-network states in loop quantum gravity: Analytical and numerical results

Eugenio Bianchi,[1,*] Pietro Donà,[1,†] and Ilya Vilensky[2,‡]

[1]*Institute for Gravitation and the Cosmos & Physics Department, Penn State, University Park, Pennsylvania 16802, USA*

[2]*Florida Atlantic University, 777 Glades Road, Boca Raton, Florida 33431, USA*

(Received 28 December 2018; published 16 April 2019)

Bell-network states are loop-quantum-gravity states that glue quantum polyhedra with entanglement. We present an algorithm and a code that evaluates the reduced density matrix of a Bell-network state and computes its entanglement entropy. In particular, we use our code for simple graphs to study properties of Bell-network states and to show that they are nontypical in the Hilbert space. Moreover, we investigate analytically Bell-network states on arbitrary finite graphs. We develop methods to compute the Rényi entropy of order p for a restriction of the state to an arbitrary region. In the uniform large-spin regime, we determine bounds on the entanglement entropy and show that it obeys an area law. Finally, we discuss the implications of our results for correlations of geometric observables.

DOI: 10.1103/PhysRevD.99.086013

I. INTRODUCTION

Elementary quanta of space—also known as quantum polyhedra [1]—are a characterizing feature of loop quantum gravity (LQG) [2–5]. These microscopic degrees of freedom (d.o.f.) are ultralocal and associated with the N nodes of a finite graph Γ. The collective state of the system is an element of the kinematical Hilbert space of the theory which, at fixed spin-network graph Γ and spins j_ℓ, has the tensor-product structure

$$\mathcal{H}_{\Gamma j_\ell} = \bigotimes_{n\in\Gamma} \mathcal{H}_n. \tag{1.1}$$

Here, $\mathcal{H}_n$ is the Hilbert space of the $SU(2)$ intertwiner associated to each node n, the quantization of a classical polyhedron [1,6–9]. This decomposition is the basis of the geometric picture of quantum space: a LQG state is a many-body state of quantum polyhedra with the adjacency relations given by the connectivity of the graph and areas given by the spins [10]. A generic state in the space $\mathcal{H}_{\Gamma j_\ell}$ is a linear superposition of quantum polyhedra,

$$|s\rangle = \sum_{i_1,\ldots,i_N} c_{i_1\ldots i_N} |i_1\rangle\cdots|i_N\rangle. \tag{1.2}$$

The factorized orthonormal basis associated to the tensor product (1.1), denoted $|\Gamma, j_\ell, i_n\rangle = |i_1\rangle\cdots|i_N\rangle$, is called the spin-network basis. This is a basis of simultaneous eigenstates of a maximal commuting set of operators that are *ultralocal*; i.e., each operator measures a geometric property of a single quantum polyhedron such as its volume or the dihedral angle between two faces [1,6–15]. As a result, spin-network basis states are factorized over polyhedra; they are unentangled. On the other hand, a typical state of this many-body system has the form (1.2) and represents entangled polyhedra.

The connectivity of the graph Γ, together with the factorized structure of the Hilbert space $\mathcal{H}_{\Gamma j_\ell}$, allows us to define regions of the graph and their associated Hilbert space. Specifically, we call A a region if the set of nodes $n \in A$ is path connected with respect to the graph structure. The associated Hilbert space is $\mathcal{H}_A = \otimes_{n\in A} \mathcal{H}_n$, and, denoting $\bar{A}$ the complement of A, we have a bipartition of the Hilbert space as the tensor product,

$$\mathcal{H}_{\Gamma j_\ell} = \mathcal{H}_A \otimes \mathcal{H}_{\bar{A}}. \tag{1.3}$$

Given this structure, it is immediate to define the entanglement entropy S_A of a pure state $|s\rangle$ restricted to the subsystem A. Let us assume that $1 \ll \dim\mathcal{H}_A \leq \sqrt{\dim\mathcal{H}_{\Gamma j_\ell}}$. In this case, Page's result [16] states that a typical state in the Hilbert space $\mathcal{H}_{\Gamma j_\ell}$ has entanglement entropy

$$S_A(\text{typical}) \approx \log(\dim\mathcal{H}_A) - \frac{1}{2}(\dim\mathcal{H}_A)^2/\dim\mathcal{H}_{\Gamma,j_\ell}. \tag{1.4}$$

This result indicates that the restriction ρ_A of a typical pure state in $\mathcal{H}_{\Gamma j_\ell}$ is close to being maximally mixed when the subsystem A is small. It is instructive to consider the case of

*ebianchi@gravity.psu.edu
†pxd81@psu.edu
‡ilya.vilensky@fau.edu

 © 2019 American Physical Society

a graph Γ that is dual to an equal-area triangulation. In this case, all spins are assumed to be equal to j_0, and the dimension of the Hilbert space of a node—an equal-area quantum tetrahedron—is simply $\dim \mathcal{H}_n = 2j_0 + 1$. The expectation value of the volume of a node is $v(j_0) = \mathrm{Tr}(\hat{V}_n \rho_n) = \frac{1}{2j_0+1}\sum_k v_k$, where v_k are the eigenvalues of the volume operator $\hat{V}_n$ and ρ_n is the maximally mixed state. When expressed in terms of these parameters, the entanglement entropy of a typical state in $\mathcal{H}_{\Gamma j_0}$ is

$$S_A(\text{typical}) \approx \frac{\log(2j_0+1)}{v(j_0)} V_A - \frac{1}{2}\exp\left(-\frac{\log(2j_0+1)}{v(j_0)}(V_\Gamma - 2V_A)\right). \quad (1.5)$$

This is a volume law for the entanglement entropy of a typical state in the Hilbert space $\mathcal{H}_{\Gamma j_0}$. On the other hand, it is known that taking into account the dynamics—and in particular constraints such as the selection of an eigenstate of a Hamiltonian with local interactions [17–19]—selects states that are nontypical in the Hilbert space and leads to a behavior of the entanglement entropy that deviates qualitatively from Page's law for typical states.

In this paper, we focus on Bell-network states and show that—instead of a volume law—their entanglement entropy obeys an area law,

$$S_A(\text{Bell-network}) \approx \frac{\log(2j_0+1)}{a(j_0)} \mathrm{Area}_A + \cdots, \quad (1.6)$$

where $a(j_0) = 8\pi\gamma G\hbar\sqrt{j_0(j_0+1)}$ is the area eigenvalue of a boundary link.

Bell-network states are defined using squeezed vacuum techniques that enforce prescribed correlations. In particular, Bell-network states [20] have correlations that reduce the general twisted geometry [21,22] at adjacent nodes to vector geometries [23,24] by introducing Bell-like correlation in the normals to faces of adjacent polyhedra. The structure of correlations is well illustrated by the Bell state for two spin-1/2 particles,

$$|\mathcal{B}\rangle = \frac{|\uparrow\rangle_1|\downarrow\rangle_2 - |\downarrow\rangle_1|\uparrow\rangle_2}{\sqrt{2}} = \sqrt{2}\int \frac{d\vec{n}}{4\pi} |\vec{n}\rangle_1 |-\vec{n}\rangle_2, \quad (1.7)$$

which is given by a uniform superposition of back-to-back spins. For a given graph Γ and assignment j_ℓ of spins, there is a unique Bell-network state in $\mathcal{H}_{\Gamma j_\ell}$, denoted $|\Gamma, j_\ell, \mathcal{B}\rangle$ here. Its expansion coefficients in the basis (1.2) are given by the $SU(2)$ symbol of the graph.

Calculating the entanglement entropy S_A of a region A of a Bell-network state is nontrivial. In this paper, we present analytical and numerical methods to compute it. We will work only with finite graphs having a finite number of nodes. The problem is structured in the same way as the standard entanglement entropy computation in many-body quantum systems, where one considers a state (e.g., the ground state of a specific Hamiltonian) and then computes the entanglement entropy for various subsystems [16–19]. In this work, we present a numerical code [25] that, for a given graph, first evaluates the expansion of the Bell-network state on a factorized basis and then computes the entanglement entropy of various subsystems. We present explicit versions of the code adapted to different graphs and subregions. We consider the dipole graph, the pentagram graph with subregions containing one or two nodes, and the hexagram graph with subregions containing one or two nodes (either connected or disconnected).

To identify qualitative features of the behavior of the entanglement entropy for any Bell-network state and arbitrary subsystem, we employ analytical methods which provide good approximations under the assumption of uniformly large spins. Under a homogeneous rescaling of the spins of the state $j_\ell \to \lambda j_\ell$, we derive a bound for the leading order in $\lambda \gg 1$ of the entanglement entropy of a region A,

$$(|\partial A| - c_A)\log\lambda \le S_A \le (|\partial A| - 3)\log\lambda, \quad (1.8)$$

where c_A is a half-integer and $|\partial A|$ is the number of links that cross the boundary of A. In this regime, the bound implies an area-law behavior for S_A. We determine also the behavior of the Rényi entropy of order p of any Bell-network state and arbitrary region. When compared to our numerical data, we find good agreement within our approximation.

The expectation that entanglement in the d.o.f. of the gravitational field is a necessary condition for the emergence of a classical spacetime is shared by various approaches to nonperturbative quantum gravity [26–34]. The result that Bell-network states satisfy an area law supports the conjecture that entanglement can be used as a probe of semiclassicality in quantum gravity [28].

The paper is structured as follows. In Sec. II, we give an elementary introduction to entropic inequalities for the entanglement entropy and the Rényi entropy, together with their application to LQG. In Sec. III, we review the definition of Bell-network states and their relation to vector geometries. In Sec. IV, we present the large-spin asymptotic analysis of the Rényi entropy and the entanglement entropy for a Bell-network state on a generic graph. In Sec. V, we present our code and compare the numerical results to our analytical asymptotic formulas for some specific graphs. We conclude with a discussion of our results.

II. ENTANGLEMENT ENTROPY AND RÉNYI ENTROPY IN LQG

A quantum system composed of two subsystems A and $\bar{A}$ has a Hilbert space given by the tensor product:

$$\mathcal{H} = \mathcal{H}_A \otimes \mathcal{H}_{\bar{A}}. \quad (2.1)$$

Given a state $|\psi\rangle$ in $\mathcal{H}$, the reduced density matrix of the subsystem A is defined by the partial trace over its complement $\bar{A}$,

$$\rho_A = \mathrm{Tr}_{\bar{A}}|\psi\rangle\langle\psi|. \tag{2.2}$$

The entanglement entropy of the subsystem A is defined as the von Neumann entropy of the reduced density matrix

$$S_A = -\mathrm{Tr}(\rho_A \log \rho_A). \tag{2.3}$$

It is also useful to define the Rényi entropy of order p, defined as

$$R_A^{(p)} = -\frac{1}{p-1}\log \mathrm{Tr}\rho_A^p, \tag{2.4}$$

with $p \geq 0$. The limit $p \to 1$ reproduces the entanglement entropy, as can be easily shown:

$$\begin{aligned}\lim_{p\to 1} R_A^{(p)} &= -\lim_{\epsilon\to 0}\frac{1}{\epsilon}\log \mathrm{Tr}(\rho_A(\mathbb{1}+\epsilon\log\rho_A)) \\ &= -\lim_{\epsilon\to 0}\frac{1}{\epsilon}\log\left(1+\epsilon \mathrm{Tr}\rho_A\log\rho_A\right) \\ &= -\mathrm{Tr}(\rho_A\log\rho_A) = S_A.\end{aligned} \tag{2.5}$$

On the other hand, the limit $p \to 0$ of the Rényi entropy reproduces the maximum entropy $S_A^{\max} = \log(\dim \mathcal{H}_A)$,

$$\lim_{p\to 0} R_A^{(p)} = \log \mathrm{Tr}\lim_{p\to 0}\rho_A^p = \log(\dim\mathcal{H}_A) = S_A^{\max}. \tag{2.6}$$

The Rényi entropies satisfy the useful inequality

$$R_A^{(p)} \leq R_A^{(p')} \quad \text{for } p > p' \tag{2.7}$$

with the equality corresponding to the maximally mixed state $\rho_A = \mathbb{1}/\dim\mathcal{H}_A$ for which $R_A^{(p)} = \log(\dim\mathcal{H}_A)$. Considering the limits $p \to 0, 1$, these inequalities provide an upper and a lower bound on the entanglement entropy,

$$R_A^{(p)} \leq S_A \leq \log(\dim\mathcal{H}_A) \quad \text{with} \quad p > 1. \tag{2.8}$$

This relation is instrumental in our analysis.

The structures discussed above apply immediately to states in the LQG Hilbert space $\mathcal{H}_{\Gamma j_\ell} = \mathcal{H}_1 \otimes \cdots \otimes \mathcal{H}_N$ with fixed graph Γ, N nodes, and fixed spins j_ℓ. In this case, a state of this many-body system is a quantum geometry consisting of N entangled polyhedra.

A similar decomposition of the Hilbert space has been used for the investigation of entanglement in the intertwiner d.o.f. in Ref. [35] and in Ref. [36], where a class of area-law states with spin $1/2$ is studied. The decomposition discussed in these works differs from the edge-mode decomposition of Refs. [37–43], where an enlargement of the Hilbert space is considered. In that case, there is a local boundary contribution due to edge modes and a nonlocal contribution due to intertwiner entanglement (quantum polyhedra). As an example of the distinction between the two definitions of entanglement entropy (intertwiner entanglement vs edge-mode entanglement), we can consider a spin-network basis state $|\Gamma, j_\ell, i_n\rangle$ and a region A. The edge-mode entanglement entropy scales as $\sum_\ell \log(2j_\ell+1)$, while the intertwiner entanglement entropy is simply zero. We refer to Ref. [44] for a detailed discussion of the relation between different definitions of the entanglement entropy in lattice gauge theory and the related choice of subalgebra of observables.

While in this paper we focus on the Hilbert space at fixed spins, $\mathcal{H}_{\Gamma j_\ell}$, the notion of entanglement entropy that we use generalizes immediately to a sum over spins. In fact, the LQG Hilbert space at fixed graph Γ does not have a tensor-product structure. It is instead given by the direct sum $\mathcal{H}_\Gamma = \bigoplus_{j_\ell}\mathcal{H}_{\Gamma j_\ell}$ over spaces at fixed spins. Remarkably, in this case, the entanglement entropy can be computed following Ref. [44]. Given a state $|\Gamma, v\rangle \in \mathcal{H}_\Gamma$,

$$|\Gamma, v\rangle = \sum_{j_\ell} q_{j_\ell}|\Gamma, j_\ell, v\rangle, \tag{2.9}$$

with $|\Gamma, j_\ell, v\rangle \in \mathcal{H}_{\Gamma j_\ell}$, the entanglement entropy of a region A can be computed as

$$S_A = -\sum_{j_\ell} p_{j_\ell}\log p_{j_\ell} + \sum_{j_\ell} p_{j_\ell} S_A(j_\ell), \tag{2.10}$$

where $p_{j_\ell} = |q_{j_\ell}|^2/\sum_{j_\ell}|q_{j_\ell}|^2$ is the probability of finding the state $|\Gamma, v\rangle$ with definite spins j_ℓ, and the entropy is the sum of the classical Shannon entropy of the probability distribution p_{j_ℓ} and the average entropy at fixed spin.

III. BELL-NETWORK STATES AND VECTOR GEOMETRIES

The LQG Hilbert space at fixed graph Γ and spins j_ℓ consist of a collection of quantum polyhedra, one for each node. Geometrical quantities like angles, areas, volumes, and shapes of these polyhedra are quantum operators in this Hilbert space. To glue two polyhedra together, we need to impose the matching of the shape of the face shared between the two. At the quantum level, due to the uncertainty relations of shape operators, we cannot require two shape eigenstates to coincide, but we can impose gluing as expectation values. Moreover, we can require correlations between two adjacent quantum polyhedra so that also the fluctuations of the shape of two adjacent faces are correlated. Bell-network states [20,31,32] are a specific proposal that uniformly maximizes correlations of all neighboring polyhedra on a given graph. They are given by the formula

$$|\Gamma, j_\ell, \mathcal{B}\rangle = \frac{1}{\sqrt{Z}} \sum_{i_n} \overline{\mathcal{A}_\Gamma(j_\ell, i_n)} \bigotimes_n |i_n\rangle, \tag{3.1}$$

where Z is a normalization and the amplitude $\mathcal{A}$ is the $SU(2)$ symbol of the graph Γ, i.e.,

$$\mathcal{A}_\Gamma(j_\ell, i_n) = \sum_{\{m\}} \prod_n [i_n]^{m_1 \cdots m_{F_n}}. \tag{3.2}$$

Here, the intertwining tensors $[i_n]^{m_1 \cdots m_{F_n}}$ are contracted according to the connectivity of the graph Γ, and F_n is the number of faces of the quantum polyhedron in the node n.

These states have an appealing geometrical interpretation: for large spins, they describe a uniform superposition of vector geometries, a collection of polyhedra glued together by requiring that the normals of adjacent faces are back to back, even though in general the faces do not have the same shape. This class of geometries plays an essential role in the study of the asymptotic behavior of topological BF $SU(2)$ spin foam vertex amplitudes [24,45–49]. Bell-network states have built-in short-range correlations and are expected to satisfy an area law for the entanglement entropy. Proving that the area law arises at the gauge-invariant level is not immediate as it requires us to control correlations in the intertwiner d.o.f. Here, we present the explicit computations necessary to determine this behavior.

While in this paper we focus on Bell-network states at fixed spins, their full definition includes also specific weights for the sum over spins. We review briefly the related construction.

Bell-network states are defined using the formalism of squeezed spin networks, developed in Refs. [31,32]. The objective is to build entangled states for neighboring quantum polyhedra.

Given a graph Γ, the Hilbert space of a link $\ell \in \Gamma$ can be thought of as the Hilbert space of four harmonic oscillators, two at the source and two at the target of the link [32]. Denoting the creation operators $a_s^{\dagger\alpha}$ and $a_t^{\dagger\alpha}$, where $\alpha = 1, 2$ is a spinor index, we build a Bell state of the link ℓ as

$$|\mathcal{B}, \lambda\rangle_\ell = (1 - |\lambda|^2) \exp(\lambda \epsilon_{\alpha\beta} a_s^{\dagger\alpha} a_t^{\dagger\beta}) |0\rangle_s |0\rangle_t, \tag{3.3}$$

where the squeezing paramenter λ is a complex number that encodes the average area A_ℓ and the average extrinsic angle θ_ℓ associated to the link. The Bell-network state of a full graph Γ is then defined as the gauge-invariant projection of the tensor product of link Bell states

$$|\Gamma, \lambda_\ell, \mathcal{B}\rangle = P_\Gamma \otimes_{\ell \in \Gamma} |\mathcal{B}, \lambda_\ell\rangle_\ell. \tag{3.4}$$

The gauge-invariant projection can be implemented using the resolution of the identity in the spin-network basis $P_\Gamma = \sum_{j_\ell, i_n} |\Gamma, j_\ell, i_n\rangle\langle\Gamma, j_\ell, i_n|$. The result of this projection takes a simple form. We obtain an expression for the graph Bell-network states in terms of a sum over spins,

$$|\Gamma, \lambda_\ell, \mathcal{B}\rangle = \sum_{j_\ell} \left(\prod_\ell (1 - |\lambda_\ell|^2) \lambda_\ell^{2j_\ell} \sqrt{2j_\ell + 1} \right) |\Gamma, j_\ell, \mathcal{B}\rangle, \tag{3.5}$$

where $|\Gamma, j_\ell, \mathcal{B}\rangle$ are the states (3.1) we focus on in this paper.

Computing the entanglement entropy of $|\Gamma, j_\ell, \mathcal{B}\rangle$ is nontrivial. Once the result of the entanglement entropy at fixed spins is obtained, the entanglement entropy of the full state can be computed using (2.10) with $q_{j_\ell} = \prod_\ell (1 - |\lambda_\ell|^2) \lambda_\ell^{2j_\ell} \sqrt{2j_\ell + 1}$.

IV. LARGE-SPIN ASYMPTOTIC ANALYSIS OF THE ENTANGLEMENT ENTROPY

Given a Bell-network state on a general graph Γ with fixed spins j_ℓ (3.1), we consider a region A containing a certain number of nodes N_A. We denote $|\partial A|$ the number of links crossing the boundary of A; see Fig. 1. The density matrix of A is defined by tracing away the intertwiners in $\bar{A}$, i.e.,

$$\rho_A = \mathrm{Tr}_{\bar{A}} |\Gamma, j_\ell, \mathcal{B}\rangle\langle\Gamma, j_\ell, \mathcal{B}| = \frac{1}{Z} \sum_{i_n, i_n'} M(i_n, i_n') \bigotimes_{n \in A} |i_n\rangle\langle i_n'|. \tag{4.1}$$

The normalization Z guarantees that $\mathrm{Tr}\rho = 1$. The matrix $M(i_n, i_n')$ is defined as

$$M(i_n, i_n') = \sum_{k_n \in \bar{A}} \overline{\mathcal{A}_\Gamma(j_\ell, i_n, k_n)}\, \mathcal{A}_\Gamma(j_\ell, i_n', k_n), \tag{4.2}$$

where the sum is over the intertwiners k_n associated to the nodes contained in $\bar{A}$, the complement of A. The normalization factor is easily expressed in terms of the matrix M as $Z = \mathrm{Tr}M$. The trace of the density matrix raised to a

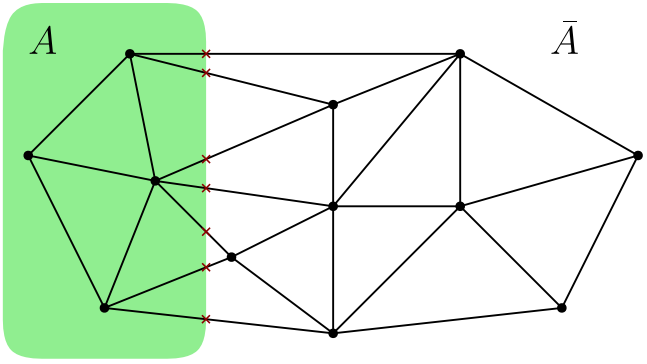

FIG. 1. Example of a general spin network on a graph Γ. We shaded in green a region A which contains $N_A = 4$ nodes and $|\partial A| = 7$ boundary links (marked with a cross). The region A determines a subsystem $\mathcal{H}_A = \otimes_{n \in A} \mathcal{H}_n$.

power p can also be expressed in terms of M as $\mathrm{Tr}\rho_A^p = \mathrm{Tr}M^p/(\mathrm{Tr}M)^p$. This formula allows us to compute the Rényi entropies in terms of the matrix M:

$$R_A^{(p)} = -\frac{1}{p-1}\log \mathrm{Tr}\rho_A^p = -\frac{1}{p-1}(\log \mathrm{Tr}M^p - p\log \mathrm{Tr}M). \tag{4.3}$$

The ingredients needed in the formula are the traces $\mathrm{Tr}M^p$. For instance, $\mathrm{Tr}M$ can be written in terms of $SU(2)$ symbols as

$$\mathrm{Tr}M = \sum_{i_n,k_n} \overline{\mathcal{A}_\Gamma(j_\ell, i_n, k_n)}\, \mathcal{A}_\Gamma(j_\ell, i_n, k_n) = Z. \tag{4.4}$$

Clearly, these quantities can be computed using $SU(2)$ recoupling theory. However, no closed expression is available, and one has to resort to numerical or symbolic codes, as the ones discussed in the next section. Here, we are interested in the behavior of the Rényi entropies under uniform rescaling of the spins. To this end, we introduce a reformulation in terms of auxiliary variables familiar in spin foam calculations. This reformulation allows us to estimate the value of the Rényi entropies analytically in the large-spin regime using a saddle-point approximation.

To write the Rényi entropies in spin foam–like variables, we express each of the $p \cdot N$ sums over intertwiners appearing in $\mathrm{Tr}M^p$ as an integral over $SU(2)$ Wigner matrices,

$$\sum_i \bar{i}_{m_1\cdots m_F} i^{n_1\cdots n_F} = \int_{SU(2)} \mathrm{d}g D^{(j_1)n_1}_{m_1}(g)\cdots D^{(j_F)n_F}_{m_F}(g). \tag{4.5}$$

The indices are contracted according to the connectivity of the graph (3.2) and result into $SU(2)$ characters. In particular, there is one $SU(2)$ character for each link crossing the boundary of A and p characters for each link completely inside or outside the region A. In total, there are $pL - (p-1)|\partial A|$ characters. By introducing a resolution of the identity in terms of $SU(2)$ coherent states $|j\vec{n}\rangle$ [50], each $SU(2)$ character $\chi^{(j)} = \mathrm{Tr}D^{(j)}$ can be expressed as an integral over a unit vector $\vec{n} \in S^2$,

$$\begin{aligned}\chi^{(j)}(g) &= (2j+1)\int_{S^2} \mathrm{d}\vec{n}\langle j\vec{n}|g|j\vec{n}\rangle \\ &= (2j+1)\int_{S^2} \mathrm{d}\vec{n}\exp\left(2j\log\left\langle \frac{1}{2}\vec{n}|g|\frac{1}{2}\vec{n}\right\rangle\right).\end{aligned} \tag{4.6}$$

The trace $\mathrm{Tr}M^p$ can then be written as an integral over $SU(2)$ group elements g_e and over unit vectors $\vec{n}_f$ as

$$\mathrm{Tr}M^p = \int d\vec{n}_f dg_e e^{f_p(j_\ell, \vec{n}_f, g_e)}. \tag{4.7}$$

The function $f_p(j, \vec{n}_f, g_e)$ is linear in j_ℓ and can be determined using diagrammatic techniques as illustrated for a specific example in the Appendix.

In the large-spin limit, the integral (4.7) can be evaluated using a saddle-point approximation. Under a uniform rescaling of all the spins $j_\ell \to \lambda j_\ell$, the function scales as $f_p(j_\ell, \vec{n}_f, g_e) \to \lambda f_p(j_\ell, \vec{n}_f, g_e)$, and the leading order in λ of the logarithm of the trace $\mathrm{Tr}M^p$ is given by

$$\log(\mathrm{Tr}M^p) = \left(\#S^2 integrals - \frac{1}{2}\#Hessian(f_p)\right)\log\lambda + O(1). \tag{4.8}$$

The first term, the number of integrals over coherent states is due to the dimensional factor $2j+1$ in (4.6). The second term, $\#Hessian$, is the rank of the Hessian of f_p, and it can be expressed in terms of the number of $SU(2)$ integrals, the number of S^2 integrals, the number of symmetries of f_p, and the dimension of the space of solutions of the system of saddle-point equations (denoted $\#space\,of\,solutions$). If multiple saddle-points exist, the dominant saddle point is characterized by the largest space of solutions. Therefore,

$$\#Hessian(f_p) = +3\times\#SU(2)integrals \tag{4.9}$$

$$+2\times\#S^2 integrals \tag{4.10}$$

$$-\#symmetries \tag{4.11}$$

$$-\#space\,of\,solutions(f_p). \tag{4.12}$$

The symmetries of f_p are related to right and left $SU(2)$ multiplication of the integration group elements g_e. It can be shown that the function f_p always has $2p$ SU(2) symmetries, resulting in $\#symmetries = 3\times 2p$. As already discussed, the number of $SU(2)$ integrals is p times the total number N of nodes of the graph Γ. Therefore,

$$\log(\mathrm{Tr}M^p) = -\frac{1}{2}(3pN - 6p - \#space\,of\,solutions(f_p))\times\log\lambda + O(1). \tag{4.13}$$

The number $\#space\,of\,solutions$ is given by the total number of independent variables (two per unit vector), minus the number of independent critical-point equations and a global rotation. In the case $p=1$, the number of independent critical-point equations coming from f_1 is $3(N-1)$ (i.e., $N-1$ vectorial equations), resulting in $\#space\,of\,solutions(f_1) = 2L - 3 - 3(N-1) = 2L - 3N$. This number appears in Ref. [24] where it is derived in the context of the asymptotic analysis of spin foam amplitudes of topological theories.

In the general case, denoting

$$C_A^{(p)} = \#\textit{redundant critical-point equations of } f_p, \tag{4.14}$$

we find that the number of independent critical-point equations of f_p is $3pN - C_A^{(p)} - 3$, corresponding to pN total vectorial equations minus the number of redundant equations ($C_A^{(p)}$) and a global rotation.

The number $C_A^{(p)}$ can be computed case by case for a given graph Γ, region A, and power p. However, a general closed formula is not available. We note that $C_A^{(p)}$ has two important properties: $C_A^{(p)}$ is an integer and is bounded from below by

$$C_A^{(p)} \geq 6(p-1), \tag{4.15}$$

which is the number of equations that are redundant because of symmetries.[1] The resulting expression is $\#space\ of\ solutions(f_p) = 2(pL - (p-1)|\partial A|) - 3 - 3pN + C_A^{(p)} + 3$.

In summary, at the leading order in λ, the Rényi entropy of a Bell-network state is

$$\begin{aligned} R_A^{(p)} &= -\frac{1}{2(p-1)}(2(pL-(p-1)|\partial A|) - 3pN + C_A^{(p)} \\ &\quad - p(2L-3N))\log\lambda + O(1) \\ &= \left(|\partial A| - \frac{C_A^{(p)}}{2(p-1)}\right)\log\lambda + O(1). \end{aligned} \tag{4.16}$$

Using the properties of Rényi entropy, we can characterize the dependence of $C_A^{(p)}$ on the order p. From the set of inequalities (2.8), we find

$$\frac{C_A^{(p)}}{2(p-1)} \leq \frac{C_A^{(p+1)}}{2p} \Rightarrow C_A^{(p)} < \frac{p}{p-1} C_A^{(p)} \leq C_A^{(p+1)}. \tag{4.17}$$

The parameter $C_A^{(p)}$ is monotonically increasing in p and, since $R_A^{(p)}$ is positive, for each $p > 1$ is bounded from above by $2(p-1)(|\partial A| - 3)$.

As discussed in Sec. II, the entanglement entropy can be obtained from the limit of $p \to 1$ of the Rényi entropy of order p. At the leading order in $\lambda \gg 1$,

$$\begin{aligned} S_A &= \lim_{p\to 1} R_A^{(p)} \approx \lim_{p\to 1}\left(|\partial A| - \frac{C_A^{(p)}}{2(p-1)}\right)\log\lambda \\ &= (|\partial A| - c_A)\log\lambda, \end{aligned} \tag{4.18}$$

where we denoted as c_A the limit $\lim_{p\to 1}\frac{C_A^{(p)}}{2(p-1)}$. This limit exists and is finite since the entanglement entropy of a system with a finite number of d.o.f. is a well-defined quantity. From the properties of $C_A^{(p)}$, we also find that

$$R_A^{(p)} \approx \left(|\partial A| - \frac{C_A^{(p)}}{2(p-1)}\right)\log\lambda \leq (|\partial A| - 3)\log\lambda. \tag{4.19}$$

Note that the inequalities here are understood as asymptotic statements holding at the leading order in $\lambda \gg 1$. Combining the limit of this inequality (that is guaranteed to exist by the monotonicity of $C_A^{(p)}$) with the most strict of the inequality in (2.8), we can determine that at the leading order in λ the entanglement entropy of a region A of a Bell-network state is bounded from below and above by

$$\left(|\partial A| - \frac{C_A^{(2)}}{2}\right)\log\lambda \leq S_A \leq (|\partial A| - 3)\log\lambda. \tag{4.20}$$

The explicit computation of $C_A^{(p)}$ requires the analysis of critical-point equations for a given graph Γ and subsystem A. However, in the special case of a subsystem A containing one single node, we can prove that $C_A^{(p)} = 6(p-1)$, which is independent of the number of boundary links. In this case, at the leading order, the Rényi entropy of order p is independent of p and (4.18), implies that $S_A = (|\partial A| - 3)\log\lambda$. This is an area law.

In general, while we do not have a closed formula for c_A, in order to show that an area law arises, we only need that c_A does not grow with $|\partial A|$. If this is the case, then—for a region with a large number of boundary links—we obtain an area law.

V. LARGE-SPIN NUMERICAL ANALYSIS OF THE ENTANGLEMENT ENTROPY

We provide a numerical code to compute the entanglement entropy and the Rényi entropy of any order of the density matrix of a Bell-network state restricted to a region A. In this section, we provide three explicit examples with Bell-network states defined on different graphs: the dipole graph, the pentagram graph, and the hexagram graph. We consider subsystems defined by regions A_i containing one or two nodes. The codes for the pentagram and the hexagram graph are available in Ref. [25].

The algorithm implemented in our C code is illustrated in the panel below (see Algorithm 1). The key ingredient of the calculation is the precomputation of all the $\{6j\}$ and $\{9j\}$ symbols needed for the evaluation of the symbol of the graph. To efficiently perform this task, we employ the WIGXJPF library and its extension FASTWIGXJ developed in Ref. [51] and previously employed in LQG computations [24,52].

[1] We note that there are $2p$ symmetries $f_p(j_\ell, \vec{n}_f, \tilde{g}_e) = f_p(j_\ell, \vec{n}_f, g_e)$ with $\tilde{g}_e = hg_e$ or $\tilde{g}_e = g_e h$ for some e, with $h \in SU(2)$. For h close to the identity, these symmetries result in a linear constraint $\delta_h f_p(j_\ell, \vec{n}_f, \tilde{g}_e) = 0$ on the critical-point equations.

Algorithm 1 Numerical algorithm for the evaluation of the Bell-network state entropy.

1: Precompute the $\{6j\}$ symbols with WIGXJPF if needed.
2: Precompute the $\{9j\}$ symbols with WIGXJPF if needed.
3: Load the symbol tables in the memory.
4: **for** each j_ℓ **do**
5: **for** each i_n **do**
6: Assemble the matrix $(\mathcal{A}_\Gamma)_{ik} = \mathcal{A}_\Gamma(j_\ell, i_n, k_n)$ with the intertwiners i_n, k_n in A, $\bar{A}$.
7: Compute the matrix $M_{ii'} = (\mathcal{A}_\Gamma^T \cdot \mathcal{A}_\Gamma)_{ii'}$.
8: Normalize it to obtain the density matrix $(\rho_A)_{ii'} = M_{ii'}/Tr(M)$.
9: Find its eigenvalues $\rho_A \to \nu_i$.
10: Compute the entanglement entropy $S_A = -\sum_i \nu_i \log \nu_i$.
11: Compute the Rényi entropy $R_A^{(p)} = -\log \sum_i \nu_i^p$.

The range of applicability of our numerical code is limited to spins up to $O(20)$ because of two factors. First, we need a considerable amount of RAM to keep accessible all $\{6j\}$ and $\{9j\}$ symbols required in the computation. For example, the computation of any symbol with spins up to 25 (both integers and half-integers) requires approximately 15 GB of available RAM, while its extension to spin 30 requires approximately 40 GB of available RAM, not commonly available on ordinary laptop computers. This obstacle can be possibly circumvented by performing a selection of the symbols prepared and loaded by FASTWIGXJ. At the present stage, we are not selecting symbols, and therefore we need to load all of them in the memory. Second, we use an array of double-precision floating-point numbers to store the symbols. Compilers generally limit the size of this array to the amount of available RAM. For example, the array of symbols for the hexagram graph occupies $(2j+1)^6 \cdot 8$ bytes. We executed our code on a machine with 16 GB of RAM; therefore, our maximum spin was limited by a hard cutoff at about $j_{\max} \approx \frac{1}{2}(\sqrt[6]{(16\ \mathrm{GB})/(8\ \mathrm{Byte})} - 1) \approx 17$.

In the following, we report the numerical computation of the entanglement entropy and the Rényi entropy of order 2 for a set of specific cases.

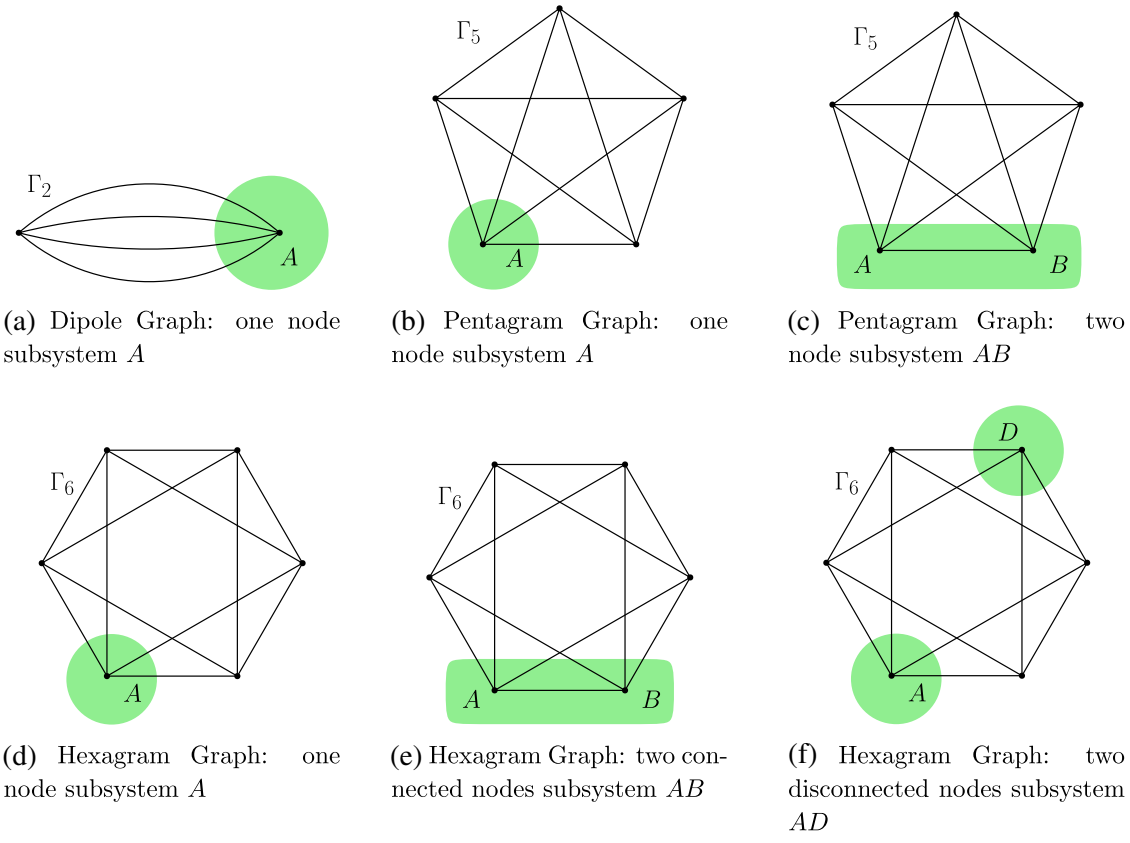

(a) Dipole Graph: one node subsystem A

(b) Pentagram Graph: one node subsystem A

(c) Pentagram Graph: two node subsystem AB

(d) Hexagram Graph: one node subsystem A

(e) Hexagram Graph: two connected nodes subsystem AB

(f) Hexagram Graph: two disconnected nodes subsystem AD

FIG. 2. Graphs and regions considered in our numerical analysis.

We set all spins equal to $j_\ell = \frac{1}{2}$ and rescale them with a parameter λ so that $j_\ell \to \lambda/2$. We will compare the numerical results to the analytical bounds derived in (4.20). We note that in all cases considered, the number of nodes in the region A is small. As a result, the bound $R_A^{(0)} = \log \dim \mathcal{H}_A$ on the entanglement entropy S_A is tighter than the bound $(|\partial A| - 3)\log\lambda$.

A. Dipole graph

The dipole Bell-network state takes a simple form, computed explicitly in Ref. [20]. In this case, analytical computations of the entropy are possible and useful for checking some of the properties derived before. We consider a dipole graph with four links [Γ_2, see Fig. 2(a)],

$$|\Gamma_2, j_\ell, \mathcal{B}\rangle = \frac{1}{\sqrt{\dim \mathcal{H}_1}} \sum_{i \in \mathcal{H}_1} |i\rangle_1 |i\rangle_2, \tag{5.1}$$

where $\mathcal{H}_1$ is the intertwiner space of a node. The two intertwiners are maximally entangled. Choosing a region A that contains a single node, the reduced density matrix is

$$\rho_A = \mathrm{Tr}_2(|\Gamma_2, j_\ell, \mathcal{B}\rangle\langle\Gamma_2, j_\ell, \mathcal{B}|) = \frac{\mathbb{1}}{\dim \mathcal{H}_1}. \tag{5.2}$$

The resulting state is maximally mixed, and all the entropies are maximal and equal to

$$S_A = R_A^{(p)} = \log \dim \mathcal{H}_1. \tag{5.3}$$

We can verify the asymptotic formula (4.16) from the exact computation in the limit of large spins. In the 4-valent case $|\partial A| = 4$, the asymptotic estimate reduces to $S_A = R_A^{(p)} = \log\lambda$, which can also be obtained from the uniform rescaling of (5.3). A similar conclusion can be reached for a dipole graph with an arbitrary number of links greater than or equal to 3.

B. Pentagram graph

The pentagram Bell-network state [see the graph Γ_5 in Figs. 2(b) and 2(c)] is a superposition of the intertwiner states weighted by the symbol of the graph, the $\{15j\}$ symbol,

$$|\Gamma_5, j_\ell, \mathcal{B}\rangle = \frac{1}{\sqrt{Z}} \sum_{i_n} \overline{\{15j\}(j_\ell, i_n)}\, |i_1\rangle|i_2\rangle|i_3\rangle|i_4\rangle|i_5\rangle. \tag{5.4}$$

One node subsystem of Γ_5. Choosing a region A containing a single node, our asymptotic formula reduces to

$$S_A \approx R_A^{(p)} \approx \log\lambda \tag{5.5}$$

at the leading order. Note that S_A and $R_A^{(p)}$ can differ by $O(1)$ terms. We used our code to compute the entanglement entropy and Rényi entropy of order 2 for all equal spins $j_\ell = \lambda/2$ and the scale parameter up to $\lambda \le 50$. We report the numerical results in Fig. 3. The plot shows clearly that S_A, $R_A^{(2)}$ and the maximal entropy $R_A^{(0)} = \log(\lambda+1) \approx \log\lambda + O(\lambda^{-1})$ differ only by a constant contribution. We interpret this $O(1)$ difference as an indication that the restriction of the Bell-network state is not maximally mixed and the state is not typical in the Hilbert space.

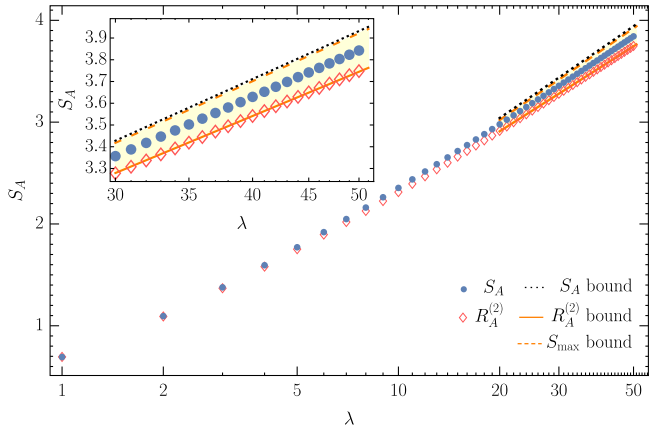

FIG. 3. [*Graph* Γ_5, *entropy of a single node*]. The figure shows our numerical results on the Bell-network state with pentagram graph Γ_5 and equal spins $j_\ell = \lambda/2$. The entanglement entropy S_A is denoted by blue dots, and the Rényi entropy $R_A^{(2)}$ is denoted by red diamonds. The lower bound asymptotic estimate is shown as a solid orange line [the $O(1)$ is fitted using the numerical data]. The upper bound estimate given by the maximal entropy is shown as a dashed orange line. We show also the bounds (4.20) as a yellow band. The inset shows the 20 data points with the largest spins.

Two nodes subsystem of Γ_5. If we choose a subsystem AB containing two nodes, our asymptotic estimates reduce to

$$R_{AB}^{(2)} = \frac{3}{2}\log\lambda + O(1) \tag{5.6}$$

and to an asymptotic band for the entanglement entropy given by

$$\frac{3}{2}\log\lambda \le S_{AB} \le 3\log\lambda. \tag{5.7}$$

For this specific configuration, the bound from above given by the maximal entropy $S_{AB} \le 2\log\lambda$ is tighter. The results of the computation of the entanglement entropy and Rényi entropy of order 2 for the case of all equal spins $j_\ell = \frac{\lambda}{2}$ and the scale parameter up to $\lambda \le 44$ are reported in Fig. 4.

C. Hexagram graph

The hexagram Bell-network state [Γ_6, see Figs. 2(d)–2(f)] is a superposition of the intertwiner states weighted by the symbol of the graph, the $\{18j\}$ symbol,

$$|\Gamma_6, j_\ell, \mathcal{B}\rangle = \frac{1}{\sqrt{Z}} \sum_{i_n} \overline{\{18j\}(j_\ell, i_n)}\, |i_1\rangle|i_2\rangle|i_3\rangle|i_4\rangle|i_5\rangle|i_6\rangle. \tag{5.8}$$

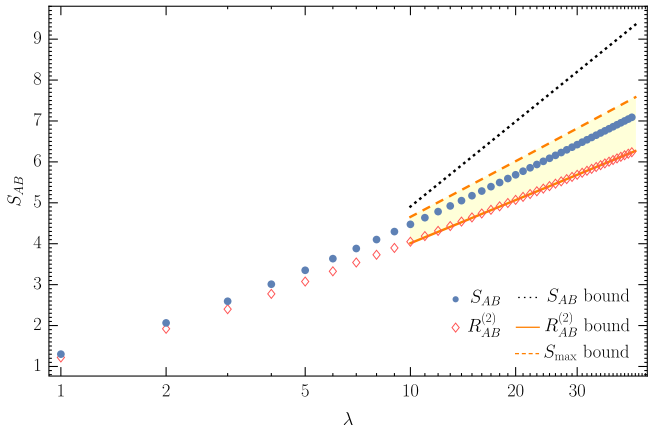

FIG. 4. [*Graph* Γ_5, *entropy of two connected nodes*]. The figure shows our numerical results on the Bell-network state with pentagram graph Γ_5 and equal spins $j_\ell = \lambda/2$. The entanglement entropy S_{AB} is denoted by blue dots, and the Rényi entropy $R^{(2)}_{AB}$ is denoted by red diamonds. The lower bound asymptotic estimate is shown as a solid orange line [the $O(1)$ is fitted using the numerical data]. The upper bound estimate given by the maximal entropy is shown as a dashed orange line. We show also the bounds (4.20) as a yellow band. Using the ten largest-spin data points, the entanglement entropy S_{AB} is fitted by $a\log(\lambda) + b + c\lambda^{-1}$ on the last ten data points obtaining $a \approx 1.94$, $b \approx -0.30$, and $c \approx 3.19$.

One node subsystem of Γ_6. Choosing a region A containing a single node, our asymptotic formula reduces to

$$S_A = R^{(p)}_A = \log\lambda + O(1). \tag{5.9}$$

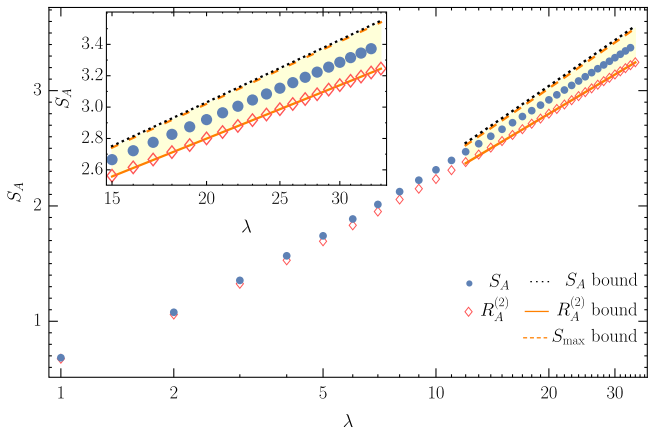

FIG. 5. [*Graph* Γ_6, *entropy of a single node*]. The figure shows our numerical results on the Bell-network state with hexagram graph Γ_6 and equal spins $j_\ell = \lambda/2$. The entanglement entropy S_A is denoted by blue dots, and the Rényi entropy $R^{(2)}_A$ is denoted by red diamonds. The lower bound asymptotic estimate is shown as a solid orange line [the $O(1)$ term is fitted using the numerical data]. The upper bound estimate given by the maximal entropy is shown as a dashed orange line. We show also the bounds (4.20) as a yellow band. The inset shows the 20 data points with the largest spins.

Note that S_A and $R^{(p)}_A$ can differ by $O(1)$ terms. As already done for the graph Γ_5, we compute the entanglement entropy and Rényi entropy of order 2 for the hexagram Γ_6 with all equal spins $j_\ell = \frac{\lambda}{2}$ and scale parameter up to $\lambda \leq 34$. We report the results in Fig. 5. The plot shows that the $O(1)$ contributions differ for S_A, $R^{(2)}_A$ and the maximal entropy $R^{(0)}_A = \log(\lambda+1) \approx \log\lambda + O(\lambda^{-1})$. We interpret this difference as an indication that the subsystem is not maximally mixed and the Bell-network state is not typical in the Hilbert space.

Two connected nodes subsystem of Γ_6. Choosing the subsystem AB consisting of two connected nodes, our asymptotic formula reduces to

$$R^{(2)}_{AB} = \frac{3}{2}\log\lambda + O(1). \tag{5.10}$$

The asymptotic band with upper and lower bounds on the entanglement entropy is given by

$$\frac{3}{2}\log\lambda \leq S_{AB} \leq 3\log\lambda. \tag{5.11}$$

For this specific configuration, the maximal entropy $S_{AB} \leq 2\log\lambda$ provides a tighter upper bound. The results of the numerical computation of the entanglement entropy and Rényi entropy of order 2 for the case of all equal spins

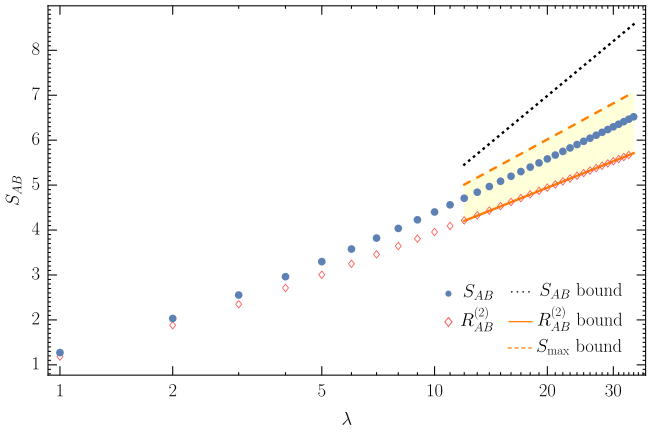

FIG. 6. [*Graph* Γ_6, *entropy of two connected nodes*]. The figure shows our numerical results on the Bell-network state with hexagram graph Γ_6 and equal spins $j_\ell = \lambda/2$, for a region consisting of two connected nodes. The entanglement entropy S_{AB} is denoted by blue dots, and the Rényi entropy $R^{(2)}_{AB}$ is denoted by red diamonds. The lower bound asymptotic estimate is shown as a solid orange line [the $O(1)$ is fitted using the numerical data]. The upper bound estimate given by the maximal entropy is shown as a dashed orange line. We show also the bounds (4.20) as a yellow band. Using the ten largest-spin data points, the entanglement entropy S_{AB} is fitted by $a\log(\lambda) + b + c\lambda^{-1}$ on the last ten data points obtaining $a \approx 1.85$, $b \approx -0.08$, and $c \approx 2.23$.

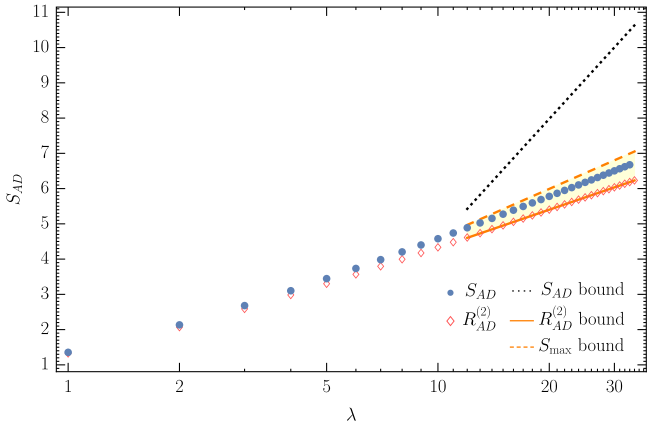

FIG. 7. [*Graph* Γ_6, *entropy of two disconnected nodes*]. The figure shows our numerical results on the Bell-network state with hexagram graph Γ_6 and equal spins $j_\ell = \lambda/2$, for a region consisting of two *disconnected* nodes. The entanglement entropy S_{AD} is denoted by blue dots, and the Rényi entropy $R^{(2)}_{AD}$ is denoted by red diamonds. The lower bound asymptotic estimate is shown as a solid orange line [the $O(1)$ is fitted using the numerical data]. The upper bound estimate given by the maximal entropy is shown as a dashed orange line. We show also the bounds (4.20) as a yellow band. Using the ten largest-spin data points, the entanglement entropy S_{AD} is fitted by $a\log(\lambda) + b + c\lambda^{-1}$ on the last ten data points obtaining $a \approx 1.86$, $b \approx 0.09$, and $c \approx 1.97$.

$j_\ell = \frac{\lambda}{2}$ and the scale parameter up to $\lambda \leq 34$ are reported in Fig. 6.

Two disconnected nodes subsystem of Γ_6. Choosing a subsystem AD consisting of two disconnected nodes, our asymptotic formula reduces again to

$$R^{(2)}_{AD} = \frac{3}{2}\log\lambda + O(1). \tag{5.12}$$

The asymptotic band providing upper and lower bounds for the entanglement entropy is now

$$\frac{3}{2}\log\lambda \leq S_{AD} \leq 5\log\lambda. \tag{5.13}$$

Again, as the subsystem still consists of a small number of nodes, the maximal entropy $S_{AD} \leq 2\log\lambda$ provides a tighter upper bound. The results of our numerical computations of the entanglement entropy and Rényi entropy of order 2 for the case of all equal spins $j_\ell = \frac{\lambda}{2}$ and the scale parameter up to $\lambda \leq 34$ are reported in Fig. 7.

VI. DISCUSSION

We studied the entanglement entropy of Bell-network states, numerically and analytically. Bell-network states were introduced in Ref. [20] as states that glue quantum polyhedra with entanglement. For given graph Γ and spin assignment j_ℓ, there is a unique Bell-network state $|\Gamma, j_\ell, \mathcal{B}\rangle$ defined by the $SU(2)$ symbol of the graph. Computing their entanglement entropy allows us to put information-theoretic bounds on correlations of shapes of adjacent polyhedra.

On the numerical side, we presented a code for evaluating the reduced density matrix of a Bell-network state and its entropy. We use the code to evaluate the entropy for small graphs containing up to six nodes. We consider various subsystems as described in Fig. 2. At a fixed graph, we studied spins ranging from $1/2$ to approximately 20. The numerical results show that Bell-network states are nontypical in the Hilbert space: We find that, at large spins, their entropy remains below by a term $O(1)$ with respect to the one of the maximally mixed state.

While the specific code used here is adapted to small graphs and large spins, a similar procedure can be adopted for general graphs.

On the analytical side, we developed methods for computing the Rényi entropy of order p for an arbitrary graph and generic region. For spins that are uniformly large, these methods provide reliable bounds on the entanglement entropy. The Rényi entropy is computed using techniques borrowed from spin foam asymptotics [23,24]; we write the trace of powers of the reduced density matrix as an integral over unit vectors and $SU(2)$ group elements,

$$\mathrm{Tr}(\rho_A^p) = \frac{\int d\vec{n} dg e^{f_p(j,\vec{n},g)}}{(\int d\vec{n} dg e^{f_1(j,\vec{n},g)})^p}, \tag{6.1}$$

where $f_p(j,\vec{n},g)$ is a linear function of all spins j_ℓ. The integral is then evaluated with saddle-point techniques under a uniform rescaling of the spins $j_\ell \to \lambda j_\ell$ with $\lambda \gg 1$. At the leading order in λ, we find that the Rényi entropy of order p is

$$R^{(p)}_A = \left(|\partial A| - \frac{C^{(p)}_A}{2(p-1)}\right)\log\lambda + O(1), \tag{6.2}$$

where $|\partial A|$ is the number of links that cross the boundary of the region A. The constant $C^{(p)}_A$ is an integer that counts the number of redundant critical-point equations for the "action" f_p. While there is no general closed formula, the number $C^{(p)}_A$ can be computed explicitly for a given graph and region, as we have done in the cases that we have studied. Moreover, using our results on the asymptotics of the Rényi entropy, we have shown that the entanglement entropy, at leading order in λ, scales logarithmically as

$$\left(|\partial A| - \frac{C^{(2)}_A}{2}\right)\log\lambda \leq S_A \leq (|\partial A| - 3)\log\lambda. \tag{6.3}$$

This result shows that, asymptotically, the entanglement entropy of Bell-network states scales linearly with the number of links $|\partial A|$ that cross the boundary of the region

A. This result can be understood as an area law for Bell-network states. To clarify this point, let us consider a graph dual to a tessellation of 3-space and a region A. The area of a face dual to a link ℓ is $a(j_\ell) = 8\pi G\hbar\gamma\sqrt{j_\ell(j_\ell+1)}$. Under a rescaling $j_\ell \to \lambda j_\ell$ with $\lambda \gg 1$, the area of the boundary of the region A can be written as

$$\mathrm{Area}_A = \sum_{\ell\in\partial A} a(\lambda j_\ell) = \langle a(\lambda j_\ell)\rangle |\partial A|, \tag{6.4}$$

where $|\partial A|$ is the number of boundary links and $\langle a(\lambda j_\ell)\rangle$ is the average area of a face. Therefore, the entanglement entropy of a Bell-network state takes the form

$$S_A(|\Gamma, \lambda j_\ell, \mathcal{B}\rangle) \approx \frac{\log\lambda}{\langle a(\lambda j_\ell)\rangle}\mathrm{Area}_A. \tag{6.5}$$

The origin of this area law is the entanglement between the shapes of quantum polyhedra.

We discuss also an application of our numerical results. For the case of a pentagram graph Γ_5, we find that the entanglement entropy of two adjacent nodes in $|\Gamma_5, \lambda/2, \mathcal{B}\rangle$ is smaller than the sum of the entropies of each node. Calling the two nodes A and B, we have $S_A \approx \log\lambda$, $S_B \approx \log\lambda$ and $S_{AB} \approx 1.94\log\lambda$ (see Fig. 4). Therefore, the mutual information $I(A,B)$ scales as

$$I(A,B) = S_A + S_B - S_{AB} \approx 0.06\log\lambda \quad \text{(Bell-network state)}. \tag{6.6}$$

This numerical result provides us with a tool to bound correlations of shapes of two adjacent polyhedra in a Bell-network state. Let us consider observables $\mathcal{O}_A$ and $\mathcal{O}_B$ which measure the shape of the quantum polyhedra A and B. In order to have correlated fluctuations of shapes [53–57], the connected correlation function

$$G_{AB} = \langle \mathcal{O}_A\mathcal{O}_B\rangle - \langle\mathcal{O}_A\rangle\langle\mathcal{O}_B\rangle \tag{6.7}$$

has to be nonvanishing. Remarkably, knowing the mutual information between A and B provides us with a bound on correlations [58,59],

$$\frac{(\langle \mathcal{O}_A\mathcal{O}_B\rangle - \langle\mathcal{O}_A\rangle\langle\mathcal{O}_B\rangle)^2}{2\|\mathcal{O}_A\|^2\|\mathcal{O}_B\|^2} \le I(A,B). \tag{6.8}$$

This relation is especially useful for a bounded operator with a known norm, as is the case for instance for the operator that measures the dihedral angle between two faces of a quantum polyhedron [13,60,61].

In the case of two quantum tetrahedra in the Bell-network state $|\Gamma_5, \lambda/2, \mathcal{B}\rangle$, our numerical result (6.6) tells us that the correlations between shapes are allowed to be nonvanishing at large spins. This result is to be contrasted to the case of the typical state in the Hilbert space $\mathcal{H}_{\Gamma_5\lambda/2}$ for which, using Page's result (1.4), we find

$$I(A,B) = S_A + S_B - S_{AB} \sim \frac{1}{2\lambda} \quad \text{(typical state)}. \tag{6.9}$$

Therefore, correlations in shapes of adjacent polyhedra are suppressed as $1/\lambda$ in a typical state but unsuppressed in a Bell-network state.

The developments presented in this paper are part of an ongoing numerical revolution in the field [52,62–65] and represent the first numerical results on the entanglement entropy of space in loop quantum gravity.

ACKNOWLEDGMENTS

E. B. is supported by the NSF Grant No. PHY-1806428. P. D. is supported by the NSF Grants No. PHY-1505411 and No. PHY-1806356 and the Eberly research funds of Penn State University. I. V. thanks Jonathan Engle and U.S. National Science Foundation for partial support under Grants No. PHY-1505490 and No. PHY-1806290. We thank Simone Speziale for helpful insights at an early stage of this work and Bekir Baytaş for useful discussions on Bell-network states.

APPENDIX: DIAGRAMMATIC METHOD TO COMPUTE f_p: A DETAILED EXAMPLE

We report here the detailed construction of $\mathrm{Tr}M^2$ for a pentagram graph and a region A containing two nodes. Using the same graphical notation used in spin foams, each green box in Fig. 8 corresponds to a $SU(2)$ integral, and each closed line corresponds to a $SU(2)$ character.

We call g_a and $\tilde{g}_a$ the group elements; j_{ab} the spin of the closed line involving the group elements g_a; and g_b, $\vec{n}_{ab}$, and $\vec{m}_{ab}$ the unit vectors used to exponentiate the characters as in (4.6).

The function f_2 defined by (4.7), $\mathrm{Tr}M^2 = \int d\vec{n}_f dg_e e^{\lambda f_2(j_\ell,\vec{n}_f,g_e)}$, is given in this case by the expression

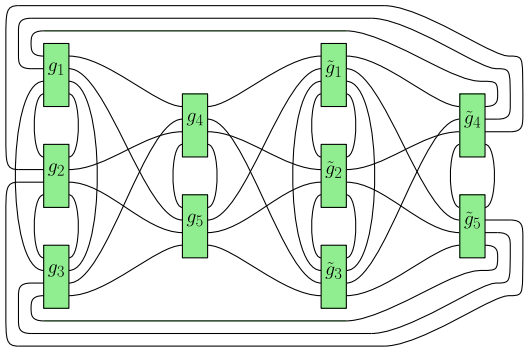

FIG. 8. Diagrammatic representation of $\mathrm{Tr}M^2$ for a pentagram graph and a two nodes subsystem.

$$f_2(j_\ell, g_n, \vec{n}_f) = \sum_{a=1}^{3} j_{a4} \log\langle \vec{n}_{a4}| g_a g_4 \tilde{g}_a \tilde{g}_4 |\vec{n}_{a4}\rangle + \sum_{a=1}^{3} j_{a5} \log\langle \vec{n}_{a5}| g_a g_5 \tilde{g}_a \tilde{g}_5 |\vec{n}_{a5}\rangle + \sum_{1\le a<b\le 3} j_{ab} \log\langle \vec{n}_{ab}| g_a g_b^{-1} |\vec{n}_{ab}\rangle + \sum_{1\le a<b\le 3} j_{ab} \log\langle \vec{m}_{ab}| \tilde{g}_a \tilde{g}_b^{-1} |\vec{m}_{ab}\rangle + j_{45} \log\langle \vec{n}_{45}| g_4 g_5^{-1} |\vec{n}_{45}\rangle + j_{45} \log\langle \vec{m}_{45}| \tilde{g}_4 \tilde{g}_5^{-1} |\vec{m}_{45}\rangle.$$

[1] E. Bianchi, P. Dona, and S. Speziale, Polyhedra in loop quantum gravity, Phys. Rev. D **83**, 044035 (2011).
[2] C. Rovelli, *Quantum Gravity*, Cambridge Monographs on Mathematical Physics (Cambridge University Press, Cambridge, England, 2004).
[3] A. Ashtekar and J. Lewandowski, Background independent quantum gravity: A status report, Classical Quantum Gravity **21**, R53 (2004).
[4] T. Thiemann, *Modern Canonical Quantum General Relativity*, Cambridge Monographs on Mathematical Physics (Cambridge University Press, Cambridge, England, 2007).
[5] C. Rovelli and F. Vidotto, *Covariant Loop Quantum Gravity*, Cambridge Monographs on Mathematical Physics (Cambridge University Press, Cambridge, England, 2014).
[6] A. Barbieri, Quantum tetrahedra and simplicial spin networks, Nucl. Phys. **B518**, 714 (1998).
[7] J. C. Baez and J. W. Barrett, The quantum tetrahedron in three-dimensions and four-dimensions, Adv. Theor. Math. Phys. **3**, 815 (1999).
[8] E. Bianchi and H. M. Haggard, Discreteness of the Volume of Space from Bohr-Sommerfeld Quantization, Phys. Rev. Lett. **107**, 011301 (2011).
[9] E. Bianchi and H. M. Haggard, Bohr-sommerfeld quantization of space, Phys. Rev. D **86**, 124010 (2012).
[10] C. Rovelli and S. Speziale, On the geometry of loop quantum gravity on a graph, Phys. Rev. D **82**, 044018 (2010).
[11] C. Rovelli and L. Smolin, Discreteness of area and volume in quantum gravity, Nucl. Phys. **B442**, 593 (1995); Nucl. Phys. **B456**, 753 (1995).
[12] A. Ashtekar and J. Lewandowski, Quantum theory of geometry. 2. Volume operators, Adv. Theor. Math. Phys. **1**, 388 (1997).
[13] S. A. Major, Operators for quantized directions, Classical Quantum Gravity **16**, 3859 (1999).
[14] B. Dittrich and S. Speziale, Area-angle variables for general relativity, New J. Phys. **10**, 083006 (2008).
[15] E. Bianchi, The length operator in loop quantum gravity, Nucl. Phys. **B807**, 591 (2009).
[16] D. N. Page, Average Entropy of a Subsystem, Phys. Rev. Lett. **71**, 1291 (1993).
[17] L. Vidmar, L. Hackl, E. Bianchi, and M. Rigol, Entanglement Entropy of Eigenstates of Quadratic Fermionic Hamiltonians, Phys. Rev. Lett. **119**, 020601 (2017).
[18] L. Vidmar, L. Hackl, E. Bianchi, and M. Rigol, Volume Law and Quantum Criticality in the Entanglement Entropy of Excited Eigenstates of the Quantum Ising Model, Phys. Rev. Lett. **121**, 220602 (2018).
[19] L. Hackl, L. Vidmar, M. Rigol, and E. Bianchi, Average eigenstate entanglement entropy of the XY chain in a transverse field and its universality for translationally invariant quadratic fermionic models, Phys. Rev. B **99**, 075123 (2019).
[20] B. Baytas, E. Bianchi, and N. Yokomizo, Gluing polyhedra with entanglement in loop quantum gravity, Phys. Rev. D **98**, 026001 (2018).
[21] L. Freidel and S. Speziale, Twisted geometries: A geometric parametrisation of su(2) phase space, Phys. Rev. D **82**, 084040 (2010).
[22] L. Freidel and S. Speziale, From twistors to twisted geometries, Phys. Rev. D **82**, 084041 (2010).
[23] J. W. Barrett and C. M. Steele, Asymptotics of relativistic spin networks, Classical Quantum Gravity **20**, 1341 (2003).
[24] P. Dona, M. Fanizza, G. Sarno, and S. Speziale, Su(2) graph invariants, Regge actions and polytopes, Classical Quantum Gravity **35**, 045011 (2018).
[25] The code presented in this paper is available at https://bitbucket.org/pietrodona/bellnetworkentropy.
[26] M. Van Raamsdonk, Comments on quantum gravity and entanglement, arXiv:0907.2939.
[27] M. Van Raamsdonk, Building up spacetime with quantum entanglement, Gen. Relativ. Gravit. **42**, 2323 (2010); Int. J. Mod. Phys. D **19**, 2429 (2010).
[28] E. Bianchi and R. C. Myers, On the architecture of spacetime geometry, Classical Quantum Gravity **31**, 214002 (2014).
[29] T. Jacobson, Thermodynamics of Space-Time: The Einstein Equation of State, Phys. Rev. Lett. **75**, 1260 (1995).
[30] T. Jacobson, Entanglement Equilibrium and the Einstein Equation, Phys. Rev. Lett. **116**, 201101 (2016).
[31] E. Bianchi, J. Guglielmon, L. Hackl, and N. Yokomizo, Squeezed vacua in loop quantum gravity, arXiv:1605.05356.
[32] E. Bianchi, J. Guglielmon, L. Hackl, and N. Yokomizo, Loop expansion and the bosonic representation of loop quantum gravity, Phys. Rev. D **94**, 086009 (2016).
[33] G. Chirco, F. M. Mele, D. Oriti, and P. Vitale, Fisher metric, geometric entanglement and spin networks, Phys. Rev. D **97**, 046015 (2018).
[34] C. Cao, S. M. Carroll, and S. Michalakis, Space from hilbert space: Recovering geometry from bulk entanglement, Phys. Rev. D **95**, 024031 (2017).

[35] E. R. Livine, Intertwiner entanglement on spin networks, Phys. Rev. D **97**, 026009 (2018).
[36] A. Feller and E. R. Livine, Entanglement entropy and correlations in loop quantum gravity, Classical Quantum Gravity **35**, 045009 (2018).
[37] W. Donnelly, Entanglement entropy in loop quantum gravity, Phys. Rev. D **77**, 104006 (2008).
[38] W. Donnelly, Decomposition of entanglement entropy in lattice gauge theory, Phys. Rev. D **85**, 085004 (2012).
[39] N. Bodendorfer, A note on entanglement entropy and quantum geometry, Classical Quantum Gravity **31**, 214004 (2014).
[40] A. Hamma, L.-Y. Hung, A. Marciano, and M. Zhang, Area law from loop quantum gravity, Phys. Rev. D **97**, 064040 (2018).
[41] F. Anz and G. Chirco, Typicality in spin-network states of quantum geometry, Phys. Rev. D **94**, 084047 (2016).
[42] C. Delcamp, B. Dittrich, and A. Riello, On entanglement entropy in non-Abelian lattice gauge theory and 3D quantum gravity, J. High Energy Phys. 11 (2016) 102.
[43] D. Gruber, H. Sahlmann, and T. Zilker, Geometry and entanglement entropy of surfaces in loop quantum gravity, Phys. Rev. D **98**, 066009 (2018).
[44] H. Casini, M. Huerta, and J. A. Rosabal, Remarks on entanglement entropy for gauge fields, Phys. Rev. D **89**, 085012 (2014).
[45] J. W. Barrett, W. J. Fairbairn, and F. Hellmann, Quantum gravity asymptotics from the su(2) 15j symbol, Int. J. Mod. Phys. A **25**, 2897 (2010).
[46] J. W. Barrett, R. J. Dowdall, W. J. Fairbairn, H. Gomes, and F. Hellmann, Asymptotic analysis of the eprl four-simplex amplitude, J. Math. Phys. (N.Y.) **50**, 112504 (2009).
[47] M. Han and M. Zhang, Asymptotics of spinfoam amplitude on simplicial manifold: Lorentzian theory, Classical Quantum Gravity **30**, 165012 (2013).
[48] J. Engle, I. Vilensky, and A. Zipfel, Lorentzian proper vertex amplitude: Asymptotics, Phys. Rev. D **94**, 064025 (2016).
[49] E. Bianchi, Spinfoam gravity, in *Loop Quantum Gravity: The First 30 Years*, edited by A. Ashtekar and J. Pullin (World Scientific Publishing, Singapore, 2017), pp. 97–124.
[50] A. Perelomov, *Generalized Coherent States and Their Applications, Texts and Monographs in Physics* (Springer, New York, 1986), DOI: 10.1007/978-3-642-61629-7.
[51] H. T. Johansson and C. Forssen, Fast and accurate evaluation of Wigner 3j, 6j, and 9j symbols using prime factorisation and multi-word integer arithmetic, SIAM J. Sci. Stat. Comput. **38**, A376 (2016).
[52] P. Dona and G. Sarno, Numerical methods for eprl spin foam transition amplitudes and lorentzian recoupling theory, Gen. Relativ. Gravit. **50**, 127 (2018).
[53] E. Bianchi, L. Modesto, C. Rovelli, and S. Speziale, Graviton propagator in loop quantum gravity, Classical Quantum Gravity **23**, 6989 (2006).
[54] E. R. Livine and S. Speziale, Group integral techniques for the spinfoam graviton propagator, J. High Energy Phys. 11 (2006) 092.
[55] E. Alesci, E. Bianchi, and C. Rovelli, Lqg propagator: III. The new vertex, Classical Quantum Gravity **26**, 215001 (2009).
[56] E. Bianchi, E. Magliaro, and C. Perini, Lqg propagator from the new spin foams, Nucl. Phys. **B822**, 245 (2009).
[57] E. Bianchi and Y. Ding, Lorentzian spinfoam propagator, Phys. Rev. D **86**, 104040 (2012).
[58] M. A. Nielsen and I. L. Chuang, *Quantum Computation and Quantum Information* (Cambridge University Press, Cambridge, England, 2000).
[59] M. M. Wolf, F. Verstraete, M. B. Hastings, and J. I. Cirac, Area Laws in Quantum Systems: Mutual Information and Correlations, Phys. Rev. Lett. **100**, 070502 (2008).
[60] R. Penrose, Angular momentum: An approach to combinatorial space-time, in *Quantum Theory and Beyond*, edited by T. Bastin (Cambridge University Press, Cambridge, 1971), pp. 151–180.
[61] R. Penrose, On the nature of quantum geometry, in *Magic without Magic* edited by J. Klauder (Freeman, San Francisco, 1972), pp. 333–354.
[62] B. Bahr and S. Steinhaus, Numerical Evidence for a Phase Transition in 4d Spin Foam Quantum Gravity, Phys. Rev. Lett. **117**, 141302 (2016).
[63] B. Bahr, G. Rabuffo, and S. Steinhaus, Renormalization of symmetry restricted spin foam models with curvature in the asymptotic regime, Phys. Rev. D **98**, 106026 (2018).
[64] B. Dittrich, E. Schnetter, C. J. Seth, and S. Steinhaus, Coarse graining flow of spin foam intertwiners, Phys. Rev. D **94**, 124050 (2016).
[65] C. Delcamp and B. Dittrich, Towards a phase diagram for spin foams, Classical Quantum Gravity **34**, 225006 (2017).